AIAA AVIATION Forum
June 25-29, 2018, Atlanta, Georgia
2018 Atmospheric and Space Environments Conference

10.2514/6.2018-3655

An Experimental Study on the Droplet Erosion Durability of a Hydro-/Ice-phobic Surface Coating

Zichen Zhang[1], Liqun Ma[2], Yang Liu[3] and Hui Hu[4] (✉)
Department of Aerospace Engineering, Iowa State University, Ames, Iowa, 50010

Icing has been widely recognized as a safety hazard for aircraft. Superhydrophobic coating surface has been proven to be effective for anti-icing applications but droplet erosion durability of the coating is not well understood which is extremely important for aircraft flying in cold and high-humidity climate. In this study, the droplet erosion durability of a commercially available superhydrophobic coating is studied. The hydrophobicity and icephobicity characteristics of the coating including contact angle, hysteresis and ice adhesion are measured after the droplet erosion experiment to evaluate the damage level of the coating. The experiment considers impact velocity and impingement times to be the variables. It was found that contact angle and hysteresis are becoming smaller after droplet erosion test and the change of hysteresis is considerably more sensitive than the contact angle (i.e., 120° variation of hysteresis and 20° change of contact angle). Impact velocity and impingement times can lead to the acceleration of coating degradation which can be observed by the change rate of contact angle and hysteresis. The source of droplet erosion damage is analyzed, and the lifetime prediction model is developed based on Corten-Dolan fatigue theory. It was found that the model can accurately predict the lifetime of the coating and can be used to theoretically compare the importance of different impact stress. The water hammer pressure and Rayleigh wave are the main factors for the coating failure.

Nomenclature

θ_c	=	Contact angle
θ_a	=	Advancing angle
θ_r	=	Receding angle
R	=	Mean radius of droplets, μm
LWC	=	Liquid water content, g/m^3
t	=	Impingement duration, s
R	=	Droplet diameter, m
ρ	=	Liquid density, kg/m3
c	=	Sound speed in liquid, m/s
ρ_1	=	Solid density, kg/m3
c_1	=	Sound speed in solid, m/s
N	=	Impingement times
n	=	Droplets numbers
P_w	=	Water hammer pressure, Pa
P_d	=	Dynamic pressure, Pa
D	=	Damage level
r	=	Damage expansion rate
S	=	Impingement area, m^2
τ	=	Ice adhesion strength, MPa
γ_{LA}	=	interfacial energy between liquid and air, mJ/m^2
γ_{IA}	=	interfacial energy between ice and air, mJ/m^2

[1] Graduate student, Department of Aerospace Engineering.
[2] Graduate student, Department of Aerospace Engineering.
[3] Post-doc Research Associate, Department of Aerospace Engineering.
[4] Martin C. Jischke Professor, Department of Aerospace Engineering, AIAA Associate Fellow, Email: huhui@iastate.edu

I. Introduction

Ice accretion presents a severe and dangerous risk for aviation security. In the cold region, when airplane takes off, super-cooled droplets in the air impinge and stick on the airfoil surface leading to the icing problem. Icing on the airfoil or engine will do considerably harm to the aerodynamic performance of airplane and probably leads to aircraft accident [1, 2]. Also, icing is more likely to happen on the wind turbine surface because wind turbines always work near the ground where air humidity is much higher than the stratosphere at which airplane works. Icing on the wind turbine will lead to the loss of energy and shorten wind turbines lifetime. To avoid icing problems, researchers have developed several techniques such as heating resistance, black paint and micro-wave radiator which are classified into active and passive way. The heating resistance, warm air, electro impulsive and using anti-freeze fluids are typical active anti-icing methods which is proven to be energy-consuming and eco-destructive. Black paint, special coating and chemicals are passive anti-icing methods which is comparatively eco-friendly. The superhydrophobic surface coating is one of the special icephobic coating based on dramatically decreasing ice adhesion forcing and repelling the incoming super-cooled-water droplets on the aircraft. Hydrophobic surfaces have achieved ultralow ice adhesion strength of 0.4 kPa which considerably reduce the difficulty of anti-icing [3].

Superhydrophobic surfaces shows poor water wettability and good repellence to water. Wettability is one of the most fundamental properties of solid surface which could be governed by the surface chemical composition and the microstructure morphology. The wing of butterfly Morpho aega [4], the feet of water starter [5] and the leaf of lotus are typical natural superhydrophobic surfaces which give people inspirations to understand the associated hydrophobic mechanism. Artificial superhydrophobic surfaces has also achieved good performance such as TiO_2 surface treated by UV illumination whose static contact angle for water is 0° and some commercial transparent superhydrophobic surfaces have been widely used in our daily life for self-cleaning and anti-fogging. The reason why coating surface presents some differences is that the surface roughness and surface energy of the coating is different. Low surface energy and high surface roughness can result in more significant hydrophobicity and vice versa. Currently, many methods have be developed to achieve rough surface such as sublimation material with silica and low surface energy can be obtained by coating special materials such as fluiroalkylsilane. One essential parameter of surface wettability is static contact angle which has commonly been used as a criterion for the hydrophobicity of surface. The contact angle is defined as the angle at which the liquid-vapor interface statically meets the solid surface. A surface exhibiting a water contact angle higher than 150° is known as super-hydrophobic surface, less than 150° but greater than 90° is hydrophobic surface and less than 90° is hydrophilic surface. The contact angle quantifies the wettability of a solid surface by a liquid via the Young's equation [6]. As the increase of contact angle, the surface topology falls into two regions, known as Cassie-Baxter and Wenzel regimes. The Cassie-Baxter state considers the effect of trapped air layer within the roughened surface whereas Wenzel state allows that water totally contact with the whole surface without air layer. Superhydrophobic surface in Cassie-Baxter state can substantially increase its contact angle and reduce sliding properties. However, the water contact angle alone is insufficient to assess the sliding properties and water resistance as a result of a totally superhydrophobic surface should have high contact angle and shows low resistance instantaneously [4]. Sliding properties of surface can be evaluated by hysteresis which is defined as the difference between receding and advancing contact angle. Advancing angle is defined as the maximum contact angle when a water droplet moves on the surface and receding angle is the minimum. Less hysteresis means less force needed to remove water from the surface so that superhydrophobic surface is widely used to self-cleaning paints, anti-fogging and anti-icing. These applications, especially the anti-icing, are very essential for aircraft and wind turbine. Roll-off angle and sliding angle also are often considered to judge the water wettability of surface.

Superhydrophobic surface is an ideal passive anti-icing technique that its ice repellent performance has been proved is effective to shrink the amount of ice accumulation. Compared with other techniques, superhydrophobic surface is low-cost, easy to maintenance, light weight and environmental friendly whereas this kind of surface will easily lose ice repellence ability after a short time use and is vulnerable to chemical corrosion, erosion and mechanical damage [7, 8, 9]. When put the surface into 5% NaCl solution, the contact angle will decrease to approximately 50° in 24 hours, which means superhydrophobic surface is totally damaged [8]. If use sandpaper to rub a pyramid-like surface on a silicon plate, a layer of material is worn off from the top of surface and although contact angle is still over 150° which means the coating is still superhydrophobic by definition, the receding angle of droplet will be zero which denotes the surface has lost water repellence ability and water will stick to the substrate [9]. Poor mechanical and chemical damage resistance is one of the most important practical limitation for superhydrophobic coating. If the surface is very delicate and unreliable, it cannot be used for the aircraft or wind turbine because working conditions of them are extremely poor as well as they need high reliability.

Droplet erosion damage regarded to be gentle and negligible compared with mechanical abrasion/friction is few considered by previous studies, while droplet impact can happen more frequently and common in our daily life. For instance, as aircraft passes through the wet cloud or takes off, a myriad of small droplets will impinge to the surface with relative high speed and could cause damage to the coating. The droplet erosion problem is found in the beginning of nineteen century when the rotating blades of steam turbines became insufficient to stand erosion damage. Basically, the water hammer effect is considered as the main damage mechanism. Exactly, at that time, the water hammer effect has been found and the solid theory has been developed by Joukowsky as he studied the valve closure failure problem in pipe flow [10]. Joukowsky think that at the moment of valve closure, the arrest of water column in the pipe will still move with initial velocity and a shock wave will be sent to the valve with sound speed which is similar to the collision of two solid metal cylinders. However, the previous droplet erosion studies are concentrated on the metal material mass loss which often happens for steam engine failure and very high-speed impingement (over 200m/s) is always needed to ruin the metal member. The evidence of metal material weaken by structural fatigue damage has been observed [11]. For current superhydrophobic coating droplet erosion experiment, the impact velocity is extremely low (no more than 20m/s) compared with previous metal erosion studies. Farhadi et al. consider supercooled droplet impingement on superhydrophobic coating but they mainly focused on evaluating coating durability with icing/de-icing cycles [12]. Wang et al. have considered low speed droplet impingement (1m/s) to the superhydrophobic coating and it shows good durability to such low-speed collision that successive droplets can rebound and roll off the surface [13]. Eric et al. used high pressure spray and water jet (15m/s) to impact the target surface and find that contact angle of the coating does not change a lot so that the surface is still superhydrophobic but water will be much easier to stick on the coating surface after impingement [14]. He also observed topology of the coating by scanning electron microscope (SEM) and do not find the difference before and after the impingement whereas chemical component change is found which is probably another main factor contributing to the droplet erosion on superhydrophobic coating. Most of studies do not tell what will affect the surface anti-icing ability and their studies are hard to be applied to the wind turbine and aircraft, since the experimental conditions are quite mild and different from the real working conditions. Therefore, it is meaningful and essential to study why droplet impact can destroy the hydro-/ice-phobicity of superhydrophobic surface and what is the primary principle of droplet erosion damage.

In the present study, the durability of a superhydrophobic coating, Hydrobead, will be studied by droplet high speed droplet erosion experiment (45m/s to 95m/s). The surface is prepared on well-polished aluminum plates. Two variables including impingement times and impact velocity will be studied as the factors to the damage of superhydrophobic surface. The research purpose is to see the effect of droplet erosion on the hydro-/ice-phobicity of the coating under different experimental conditions.

II. The droplet erosion model on the surface

Before talking about the durability test about the coating, the mechanism of droplet erosion needs to be seriously considered to provide solid theoretical foundation to experiments. As illustrated by Thomas et al., in the impact between a liquid drop and a solid surface, the initial violent load normal to the coating surface and the shear stress exerted on the surface by rapid flow away from the impact area are generally considered as two main factors contributing to the deformation of solid surface [11]. The rapid lateral flow will not be considered in this paper because the duration of it is very short and liquid impact at the initial stage is comparatively important to the surface damage [15]. The initial normal load is usually water hammer pressure which is firstly estimated by Cook and latterly, in 1933, Haller considered the compressibility of solid into the Cook's result and got the generally used water hammer pressure. The Haller's equation is given by:

$$P_w = \rho c v \left(\frac{1}{1+(\rho c/\rho_1 c_1)}\right) \tag{1}$$

Assumed a water drop impinging on an aluminum surface with a velocity of 65m/s, the water hammer pressure is approximately 85MPa which is lower than the yield strength of aluminum but is harsh enough to make some change on the surface. If a water drop impinges on a Polymethyl methacrylate (PMMA) with the same velocity, the impact pressure is only nearly 60MPa which is much lower than the pressure on aluminum surface because water hammer pressure needs to be determined with target surface properties. Water hammer theory simplifies the drop impingement phenomenon by assuming the pressure is uniform around the impact center, while pressure in that area will change with the propagation of shock wave. The most comprehensive treatment to date for a liquid drop impacting a rigid

surface is the geometrical acoustics model of Lesser which can give the detailed pressure field in the contact area [16]. However, water hammer pressure gives a simple but accurate calculation about the drop impingement stress and will be mostly considered in this paper. Equation (1) shows that the magnitude of impact pressure is independent of the geometry and size of the drop whereas the contact area experiencing this pressure relates to the size of drop and is given by $r' = Rv / c$ where R is the radius of drop.

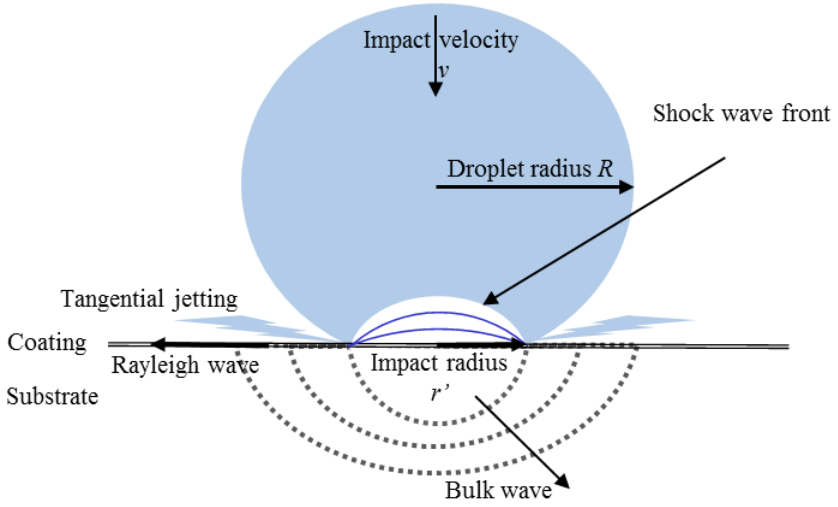

Figure 1: Droplet impact and wave propagation

In physics, every disturbance on a surface can generate a surface wave that propagates along the interface between different media. A typical example is gravity waves along the surface of ocean and the earthquake Rayleigh wave on the earth. As a result, bulk waves and Rayleigh wave are immediately generated and propagates along the interface and also in the body. Figure 1 shows the overview of droplet impact and generated waves propagation. The waves' amplitude attenuation on the surface is only considered in this paper because the damage of superhydrophobic coating rather than the substrate is principally concerned. Damping of the waves is related to the distance from the impact center according to Slot et al. [7]. Bulk waves will decay with $1/r^2$ at the surface which is much stronger than damping of the Rayleigh wave who decays with $1/\sqrt{r}$. The calculation equation of Rayleigh wave is given as equation (2) where the distance from the center is normalized by the water hammer contact area radius r' to ensure the correctness of unit and stress continuity at the edge of contact area. Bulk wave's magnitude reduces much faster than the Rayleigh wave. For instance, assuming a water drop impacting on an aluminum with a velocity of 65m/s, when wave propagates to $r=3r'$, the Rayleigh wave's amplitude is 50MPa, but the amplitude of bulk wave is only one fifth of it, 10MPa. Higher wave amplitude represents more severe damage that can be caused. Therefore, Rayleigh wave can be the dominated disturbance in the far field and the damage of the bulk waves is ignored due to its fast decay rate.

$$P_w(r) = \rho c v \left(\frac{1}{1+(\rho c/\rho_1 c_1)}\right)\left(\frac{r}{r'}\right)^{0.5} \tag{2}$$

After the initial compressible stage, release wave will come to the impact center which leads to the pressure dramatic drop and theoretically, by momentum conservation law, the maximum pressure at this stage is approximately ρv^2 which is given by equation (3) and has been observed by experiment [15]. Soto et al. measured the impact force of a dropping Galinstan and water droplet and the result can be well predicted by $F=\rho v^2 \pi R^2$ which can be regarded as a dynamic pressure ρv^2 applied over a surface area πR^2. Dynamic pressure is much weaker than the water hammer pressure or even Rayleigh wave pressure. If a water impact on an aluminum surface with a velocity of 65m/s, the dynamic pressure is nearly 4MPa which is only 5 percent of water hammer pressure, but the dynamic pressure can be effective on a much larger area whose radius is R, tens of times of the water hammer pressure radius. The massive increase of area can lead to the increment of degradation possibility. Meanwhile, former studies about the droplet erosion usually concerned the mass loss of metal material which requires the impact stress should be at least higher than the fatigue limit (138MPa, aluminum) of metal. However, the mechanical characteristics of the superhydrophobic coating is unknown and mass loss cannot be observed for this coating. Therefore, dynamic pressure needs to be properly considered.

$$P_d = \rho v^2 \tag{3}$$

Thomas et al. uses repeated impact apparatus to find the relationship between the impact cycles and the damage level of surface [11]. Their apparatus is a rotating disk which is put in a high-humid chamber so that they can calculate the impact times by recording rotating cycles, while this method does not work well if *LWC* is taken into consideration because higher *LWC* can contribute to more severe damage in the same time and different cases cannot be equally compared. It is much fairer to consider the number of single droplet impact, since more factors such as time, *LWC* and impact velocity are included properly and can be compared equally. If droplets are perfectly sphere and their size equals to mean diameter, the impingement times' calculation can be given by:

$$N = \frac{n\pi R^2}{S} \tag{4}$$

This impingement times is the ratio of the sum of droplets cross-sectional area and the area of the impingement region which can reveals the impingement times on a unit area. If two experiments have the same *N*, the amount of impact droplets can be the same which can reduce the uncertainty of experiment. *N* is calculated based on the impact area of dynamic pressure rather than the water hammer pressure, since all three illustrated stresses will be applied on the surface for one single impact and can be regarded as a stress cycle in total. Hence, the maximum impact area during the considered impingement process is thought to be the effective area. The number of droplets, *n*, is related to the experiment duration, *LWC* and wind velocity which can be expressed by:

$$n = \frac{LWC \cdot t \cdot v \cdot S}{\frac{4}{3}\rho\pi R^3} \tag{5}$$

v is the outlet wind speed. The number of droplets *n* is calculated by the ratio of total mass of impingement water and the mass of a single droplet. Substituting *n* in equation (4) can get the relationship between impingement times *N*, *LWC*, impingement duration *t* and impingement velocity *v*:

$$N = \frac{3LWC \cdot t \cdot v}{4\rho R} \tag{6}$$

The impingement times can be regarded as a nondimensional number combined *LWC*, *t* and *v* and conceptually, this number has close relationship with impingement duration in this experiment. If the water amount sprayed from the nozzle is a constant, LWC is proportional to 1/*v*, so that the multiplication of *LWC* and *v* is a constant, $LWC \cdot v = C$ (*C* is a constant) and the only variable left is impingement duration *t*. In this experiment, the water amount from the nozzle does not change by making provided water pressure and air pressure be a constant and as a result, droplets impingement times *N* can substitute the impingement duration. However, it is still significant to introduce impingement times *N* because experiment results can be equally compared.

III. Experimental Setup

Figure 2(a) shows the droplet erosion experiment setup. The durability test is conducted with an open wind tunnel which can accelerate the spray droplets driven by a high thrust electric ducted fan (EDF, JP Hobby 90mm 12 blade metal) at the end of wind tunnel. The wind speed at the wind tunnel outlet is measured by a Pitot tube which can vary from 40m/s to 95m/s and distance from wind tunnel outlet to the test plate is 50mm. The diameter of wind tunnel outlet is *l*=38mm (1.5 inches). A nozzle (IKEUCHI BIMV-11002 fog nozzle) in the wind tunnel middle section can spray droplets 20-100μm in diameter in flow direction. This nozzle is designed to mix compressed air and water inside the nozzle that air flows into the center of the nozzle, while water goes along its circumference so that droplets are sprayed forward rather than swirling. Therefore, external high-pressure air and water are necessary for the generation of spray and will control the mean diameter of spray droplets and LWC at the outlet. BIMV-11002 nozzle is selected for this study, since it is widely used in Iowa State Icing Research Tunnel and the diameter of spray droplets has been accurately measured by phase Doppler particle analyzer (PDPA). This kind of nozzle can stand maximum 60psi water and air pressure and its minimum working pressure is 30psi. Deionized (DI) water is used in this study to eliminate the erosion to the nozzle. This wind tunnel can give an *LWC* 15g/m^3 at the outlet with a velocity of 65m/s. Droplets will move nearly 1 meter in the wind tunnel before impacting on the target plate where the size of droplet may significantly change. Hence, it is necessary to measure the diameter at the outlet. The size of droplet is measured by shadowgraph technique which uses a high-speed CCD camera (PhotronFastCam MINI WX100) to record the shadow of droplets with bright light background provided by powerful LED lamp (Veritas miniConstellation 120 28°) to

increase signal-noise ratio. Droplet pictures are analyzed by Lavision ParticleMaster software to get the sizes of droplets. Figure 2(b) and 2(c) reveal the PIV measurement results with a freestream velocity of 65m/s and a test plate put at the downstream 33mm from the outlet. A highly uniform flow field can be seen near the outlet in figure 2(b) as well as flow would slow down as approaching the test plate due to increasing pressure drag. Figure 2(c), which shows the x-component velocity on the dash line in figure 2(b), uses the velocity normalized by freestream velocity to show the uniformity of flow field and tiny change of velocity.

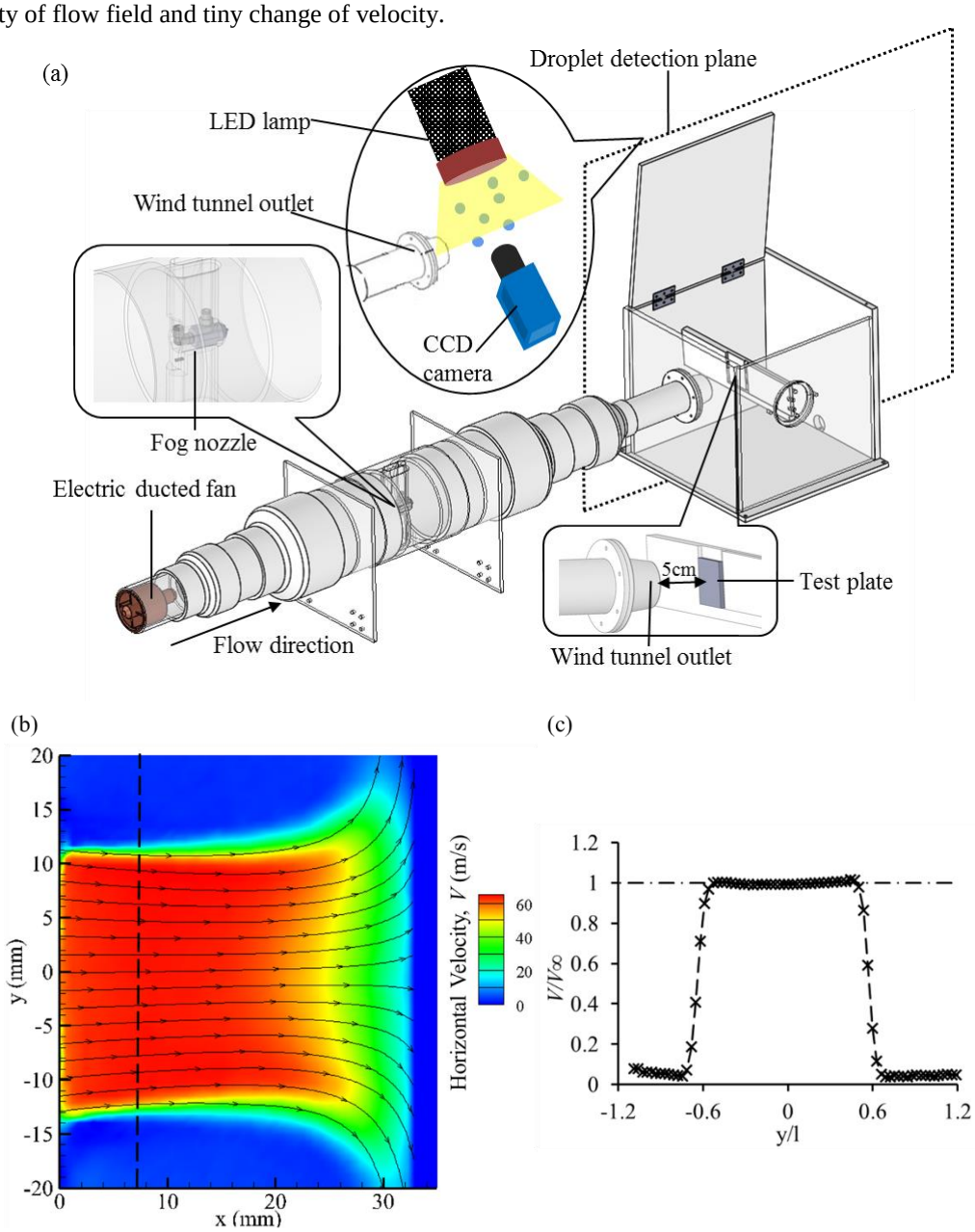

Figure 2: (a) Droplet erosion wind tunnel and droplet size measurement setup; (b) horizontal velocity profile at tunnel outlet with a freestream velocity of 65m/s; (c) horizontal velocity on the dash line in figure 2(b) at x=0.2l

Measurement setup of CA and hysteresis is shown in figure 3. High-speed camera (PCO 1200hs camera) is controlled by the delay generator (Stanford DG535 delay and pulse generator) to record droplet movement with a constant frequency (15Hz). The recorded pictures are exhibited in figure 3 and will be analyzed by ImageJ commercial software to get the angle at the contact line. Syringe pump (Genie Touch syringe pump) is used to squeeze or loose a specific volume water in a constant time. 10 μL DI water is squeezed for contact angle measurement and 50μL DI water will be squeezed and retracted in 5 seconds to do hysteresis measurement. Droplet contact angle at both sides

will be measured and the average of them is used as the contact angle of the droplet. The maximum dynamic contact angle during the squeezing period is recorded as the advancing angle and the minimum during the retracting process is considered as the receding angle of coating. CA and hysteresis measurement will be repeated at least three times for each experimental case to eliminate random error of the measurement.

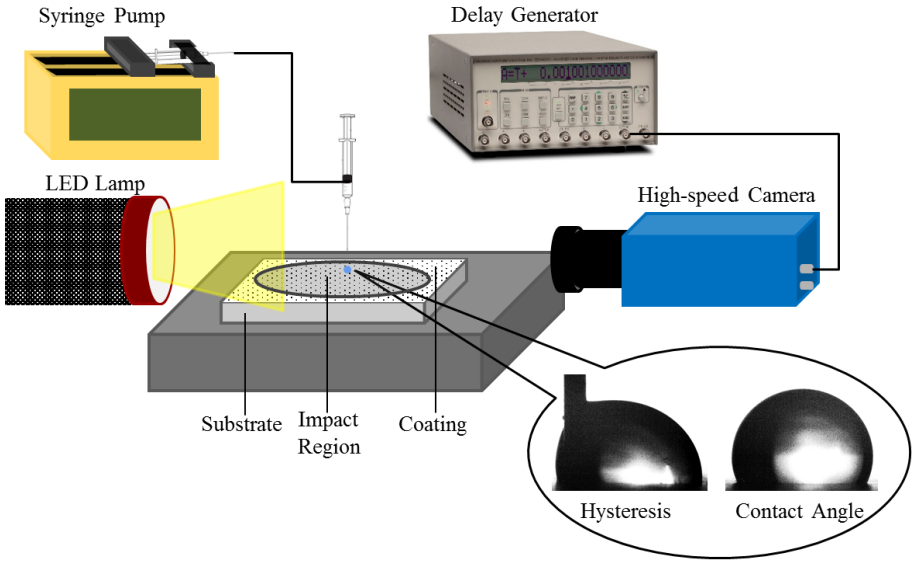

Figure 3: Contact angle and hysteresis measurement setup and example

Figure 4 presents the ice adhesion strength measurement apparatus which will be used after CA and hysteresis measurement. Meuler et al. use similar apparatus to measure ice adhesion stress with many metal and composite materials and get quantitatively meaningful results [17]. The test plate will be put into a climate chamber where housed with low-humidity CO_2 generated by dry ice to prevent frost over the test surface and cooler. A 3-D printed hollow cylinder sample made with ViewWhite plastic material whose diameter is 11mm is used to contain DI water during the icing period and hold ice. The cylinder sample is put in the impingement area and 0.5ml DI water is infused into it. The temperature in the climate chamber is controlled by a Peltier cooler (TETech CP-061) which is controlled by an external digital thermal controller (TETech TC-48-20) and can be achieved to -20°C under ambient room temperature. Temperature will be fed back by a thermistor sensor (MP-3193) which locates on the Peltier cooler. In this paper, temperature will down to -10°C and stabilize for 15 minutes allowing the water to be fully frozen under the determined temperature. A force gauge (Mark-10 series 4) is implemented on a linear actuator (Newport CONEX-LTA-HS) and will move at a rate of about 0.5mm/s until the cylinder sample is sheared of the surface. The sample rate of force gauge is 22000 samples/s which is high enough to get the peak force considered as the ice adhesion force.

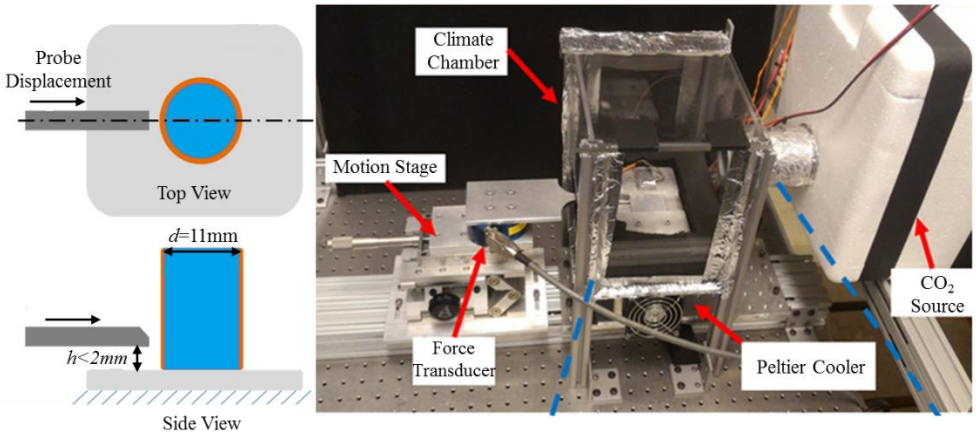

Figure 4: Ice adhesion strength measurement setup

Superhydrophobic coatings are made by spraying commercial coating (Hydrobead) on well-polished aluminum plates. Aluminum is polished with sandpaper grits ranging from 220 to 2000 and further with polishing compound to achieve mirror [18]. This kind of surface is inspired by the surface of lotus and can construct a kind of special nanostructure on the surface to achieve the superhydrophobic purpose. The Hydrobead standard is sprayed uniformly and after 20 minutes drying, Hydrobead enhancer is sprayed on the test plate which can highly improve the coating hydrophobic and icephobic durability. The distance from the spray gun to the target surface is a constant 9 inches to eliminate the difference of coating surface.

IV. Results and discussion

A. superhydrophobic coating surface droplet erosion durability

Usually, droplet erosion test needs to be conducted for steam turbine or wind turbine, since their rotating speed is extremely high (over 1 Mach) and they need to work under high humidity condition. The previous studies have several parameters to evaluate the damage of surface: the first one is the mass loss rate of material [11], the second is the maximum erosion depth [7, 19] and the incubation period duration which is defined as the time length before the mass loss is also considered. However, superhydrophobic coating droplet erosion durability test is different from the typical droplet erosion test because previous studies mostly concentrate on the failure of metal surface which can contribute to the break of steam turbine, while test in this paper particularly wants to find the decrease of coating hydrophobicity and icephobicity. Therefore, it is very important to find other criterions for judging the failure of superhydrophobic coating. There are also many considerations about the durability of hydrophobic coating: contact angle, hysteresis, ice adhesion stress, topology by AFM/SEM, sliding angle and chemical component [12, 13, 14, 20, 21, 22]. Hysteresis can show the sliding property of coating as well as the sliding angle and chemical components of Hydrobead is unavailable because of commercial confidentiality. Hence, contact angle hysteresis, topology and ice adhesion are selected to be characteristics of evaluating coating damage level.

Figure 5 presents the effect of droplet impact on contact angle of each wind speed ranging from 45m/s to 95m/s. The sliding performance of the sample after droplet erosion test is shown in figure 6. Impingement times and duration are shown in both figures to provide effective ways for comparing results with different experimental conditions. Symbols represent the experimental data and the dash line curve is the trend line of the data. The experiment will be stopped when hysteresis of the coating stops growing or significantly slowing down growing rate because the coating surface has completely lost its original hydrophobicity characteristic at that moment which is also acknowledged by Xiu et al. as they study the mechanical abrasion durability of superhydrophobic surface [9]. The surface failure will be further investigated in next following coating lifetime section.

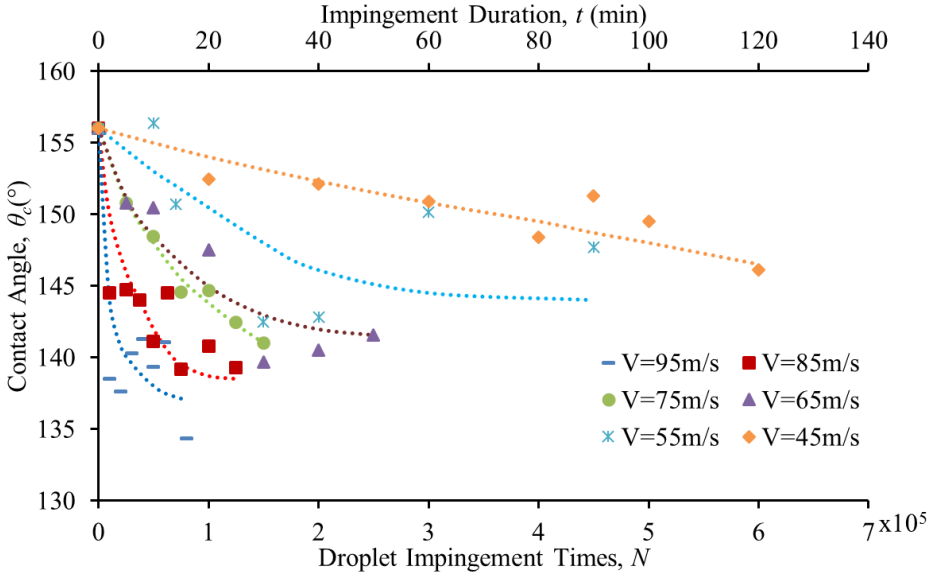

Figure 5: Variation of contact angle with droplets impingement times for different wind velocity

As for the contact angle, before spraying, each sample can show a contact angle of 156° ± 2° which well meets the result of previous studies[14, 18]. After spraying, comparing the data under one specific wind speed, descendant trend of contact angle with increasing droplet impingement times can be observed in all experiment sets but the change of contact angle is not very considerable, especially under low wind speed. Meanwhile, after the impingement, although the coating is not superhydrophobic anymore, it is still hydrophobic which means the coating can be partially effective on well-polished aluminum substrate whose contact angle is nearly 68° [18]. For the case with a velocity of 45m/s, the sample lost its superhydrophobic performance (CA>150°) until impingement times reaches 5×10^5 but as wind speed increases to 95m/s, the coating's contact angle directly decreases to 140° after 10^4 impingement which means that high wind speed can accelerate the degradation of the coating. This regulation also can be seen for other cases. Except higher degrading rate, high wind speed case is noticed more severe damage, since the contact angle of it becomes much smaller. For example, when impact velocity is 45m/s, the contact angle only changes about 9° dropping to 147° and as the speed grows up to 95m/s, contact angle of coating can reach to 135° which is achieved with shorter impingement duration.

The non-damaged coatings have a stable hysteresis of 5° ± 2°, while hysteresis changes much more significantly and regularly than the contact angle. Hysteresis of each case will dramatically increase at the beginning and the increasing rate will gradually go down to zero where hysteresis curve become a plateau. The mildest case with a velocity of 45m/s can have a maximum hysteresis approximately 75° after 4.5×10^5 impingement times and the experiment with 95m/s velocity can observe a maximum hysteresis nearly 120° which is 24 times of the initial hysteresis and 45° bigger than the mildest case. The maximum hysteresis will increase with the increase of the impact velocity, especially for high speed cases and the degradation rate also grows up as wind speed increasing. The change of hysteresis has no need to couple with the contact angle [14]. The advancing angle for all experiment cases mostly keeps being a constant, 165° ± 5° so that the variation of hysteresis can mainly reflect the change of receding angle which closely relates to the adhesion stress of liquid water and ice. Advancing angle is related to the energy needed to bring the surfaces together and receding angle reveals the energy for surface separation [23]. Consequently, droplet erosion on this superhydrophobic surface contributes to the considerably increase of ice and liquid water adhesion stress and reduces the water repellence and anti-icing performance of the coating which is unacceptable for ice mitigation purpose. This is the reason of stopping experiment as hysteresis reaching a plateau. Although coating can be totally removed after a very long-time erosion, the superhydrophobic surface has substantially lost its functions after the initial fast degradation.

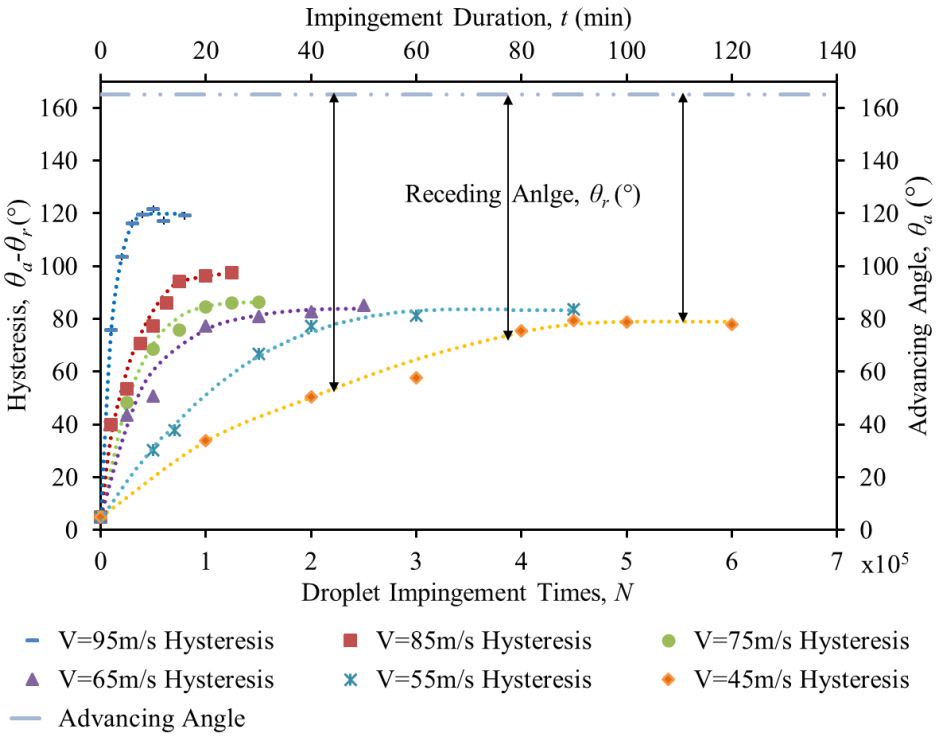

Figure 6: Droplet impact effect on hysteresis and advancing angle with different impact velocity, impingement times and duration.

Hydrophobicity performance of the coating become worse with the rise of impact velocity and duration which is also observed by Alexander used the same coating to do the similar experiment with much lower impact velocity (15m/s) [18]. He would like to contribute the damage to the water saturation of the micro-textured surface rather than mechanical erosion because he observed that contact angle returns to the initial value after drying the saturated water and SEM images of him show the tiny change of surface topology. Considering his gentle experimental conditions that directly spraying fog-sized droplets to the test plate with maximum 15m/s, his conclusion is limited to our result because the wind speed in this experiment can be much higher than him. In another aspect, his explanation also cannot give a right answer about worse sliding properties of the coating after spraying. However, his exploration gives us some inspirations about analyzing our experimental results. Firstly, contact angle of coating is less sensitive than the hysteresis to droplets erosion which also can be seen in current result that contact angle variation is nearly 20° but the hysteresis variation is 120°. It has been shown that increased roughness is critical for an increased contact angle. Droplet erosion may change the topology of the original coating and make the surface to be non-sequential, but it cannot considerably change surface roughness, while the change of surface topology can lead to the change of wetting state from Cassie-Baxter state to Wenzel state where water can have more contact area with the coating. Secondly, surface topology needs to be considered and observed to reveal the destruction of droplet erosion.

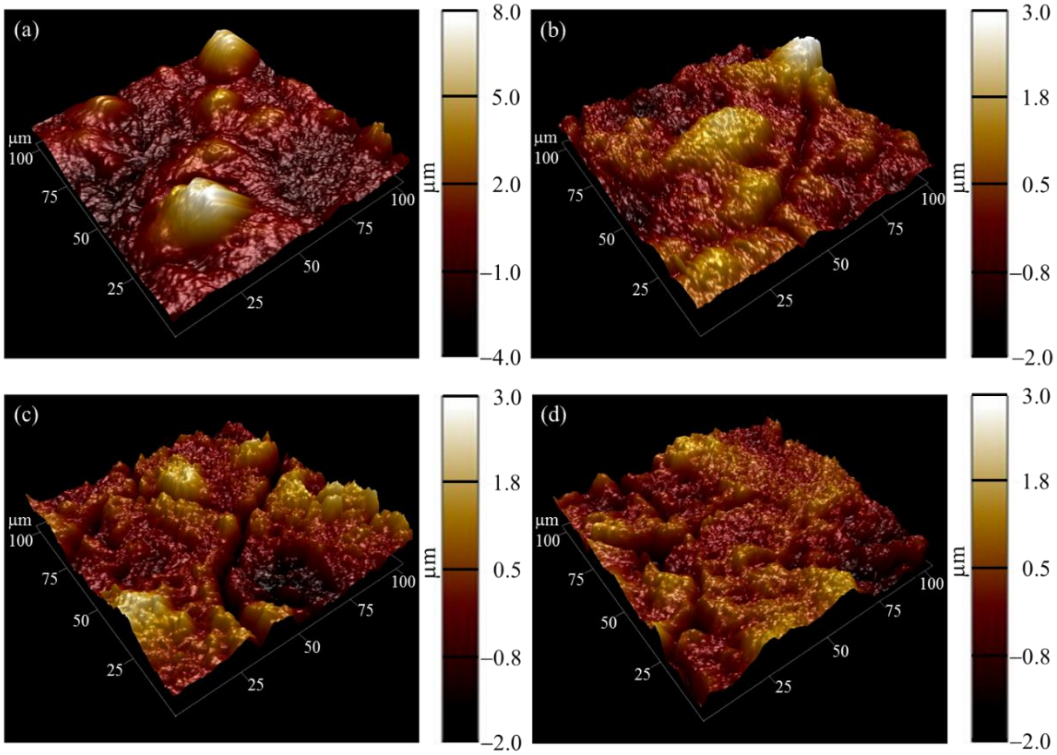

Figure 7: AFM surface topology images of superhydrophobic coating after droplets impingement with a velocity of 65m/s with different impingement times: (a) non-damaged; (b) 0.5×10^5; (c) 1.5×10^5; (d) 2.5×10^5

Figure 7 shows AFM scan surface topology images of the coating. Figure 7(a) shows non-damaged coating that has a Ra of 1219nm, which is rough enough to construct a superhydrophobic coating. In figure 7(b), after 10 minutes impingement with a velocity of 65m/s, Ra dramatically decreases to 501nm which is less than half of the non-damaged coating. Small Ra leads to poor hydrophobicity of coating and the contact angle and hysteresis in figure 5 and figure 6 has a considerably change. Contact angle drops to 149° from 156° and hysteresis increases by 40°. The Ra of figure 7(c) is 517nm which is not very different to the former stage and this is unreasonable because the coating hydrophobicity becomes worse. However, the small bulges in figure 7(b) disappear in figure 7(c) which means the coating material is removed during this period and the coating becomes flatter. The dark region in which could be coating surface defects in figure 7(c) is most possible to explain the higher roughness. Figure 7(d) is the topology after 60 minutes impingement and has Ra of 425nm which is a little lower than figure 7(c). The hydrophobicity performance of it is almost equal to the 30 minutes and hysteresis is higher than that. AFM images help people to observe the nano-

scale surface topology which can reflect the micro difference between coatings. After impingement, surface becomes flatter and coating material is removed gradually.

The wettability of substrate can be regarded as the free energy associated with the formation and elimination of interfacial areas. Meuler suggests that work of adhesion of liquid water has close relationship to the receding angle [17]:

$$W_p = \gamma_{LA}(1+\cos\theta_{rec}) \tag{7}$$

W_p is called practical work of adhesion. At the right side, the first term is the effect of liquid and air interaction and the second in the bracket provides the solid and liquid interaction. As a result, if the temperature does not change, the first term is a constant for a specific liquid, but the liquid-solid interaction is more complicated due to the complexity of solid surface. However, receding angle on the surface can give us an estimation about the liquid-solid interaction. It is reasonable because if a droplet needs more energy to be removed from a surface, the deformation of it can be larger which contributes to a higher receding angle. If the energy of fracture is known, the adhesion stress can be given by Griffith's fracture theory:

$$\tau = (\frac{EG}{\pi a})^{0.5} \tag{8}$$

E is the Young's modulus of ice; G is the fracture energy and a is the crack length. The theoretical crack length is the quarter of the diameter of the ice sample. The energy calculated by equation (7) is the for liquid water but Meuler et al. has proven the ice adhesion also have close relationship to liquid-solid interaction [17]. Hejazi et al. use energy between ice and air γ_{IA} to substitute the liquid-solid interfacial energy in equation (7) and get a satisfied result [23, 24]. The ice adhesion stress is estimated by equation (9):

$$\tau = (\frac{2E\gamma_{IA}(1+\cos(\theta_{re}))}{\pi a})^{0.5} \tag{9}$$

The theoretical prediction of ice adhesion stress and the experimental results are shown in figure 8. The tested sample is conducted droplet erosion experiment with 85m/s and 65m/s wind velocity and by controlling the impingement times, the receding angle on the surface can be achieved to a specific value. The average adhesion stress of two-cylindrical samples locating in impingement area center represents the ice adhesion strength value of the tested coating surface. In the calculation, the Young's modulus of ice is 8.7×10^9 Pa and the ice-air interaction energy is 109mJ/m^2 [25]. The results can have a same trend as the predicted curve which means the tested results are reasonable. The uncertainty may come from the selection of parameter, since the interaction energy used in this study is measured under 0 degree Celsius which is widely used as the ice-air interfacial energy. It is interesting that ice adhesion stress of the superhydrophobic surface can be comparatively accurately predicted by the theory, but other results is a little higher than the theoretical value. One possible explanation is that for non-damaged coating, the wetting state is still Cassie-Baxter state which considerably reduces the contact area of ice and solid surface by introducing the air voids whereas after droplet erosion, the wetting state transfers to Wenzel state gradually and therefore ice adhesion becomes stronger due to big contact area. With the increase of receding angle, ice adhesion will also increase which notices the icephobicity of the coating is becoming worse. Due to the monotonically increasing of receding angle with more impingement times, the droplet erosion will lead to the degradation of coating icephobicity.

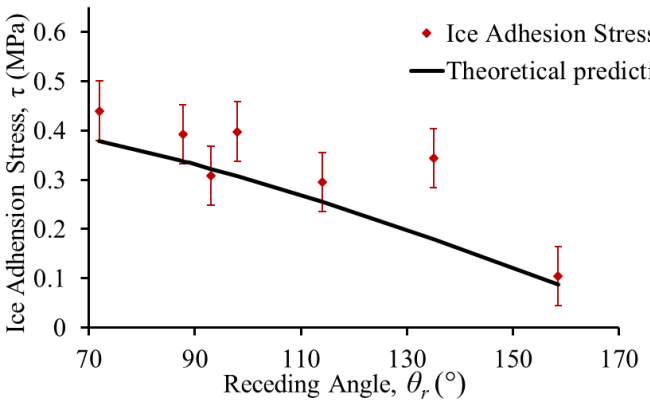

Figure 8: averaged strength of ice adhesion measured at -10°C for the superhydrophobic coating against water receding angle.

B. Coating lifetime model based on material fatigue theory

The superhydrophobic surface durability has been studied widely but the relationship between experiments conditions and practical application conditions is not properly analyzed. If such relationship can be developed, people can use relatively simple apparatus to study complicated and tough problems. In this experiment, the wind velocity is only up to 95m/s which is a little lower than the commercial aircraft cruise velocity, which indicates that it is necessary and significant to find a method to predict the coating durability on aircraft under current experimental conditions. Water hammer pressure, Rayleigh wave and dynamic pressure are considered for the damage of superhydrophobic coating in section II. Concerning the damage mechanism, previous studies intelligently put up an idea that fatigue could be one of the degradation methods of droplet erosion from a consideration of the impact conditions. Fatigue is defined as an accumulated damage in which material property deteriorates under repetitive loading [11]. The loading of droplet erosion is repetitive which can be shown by impingement times' calculation and the damage of the coating which can be reflected by hysteresis gradual increase is an accumulated procedure. Meanwhile, fatigue deterioration is a kind of permanent damage which is also observed by AFM surface topology in figure 7 where original small bulges are removed by droplet erosion. Except the repetitive loading and accumulated and permanent damage, high impact pressure and stress concentration contributed by surface roughness also can promote the fatigue damage of droplet erosion. Therefore, a fatigue model for coating lifetime prediction will be suitably tried to develop. Applied stress, number of stress cycle and failure judgement need to be determined before model development. The three stresses discussed in section II are combined as a stress spectrum in one stress cycle and the number of cycle is equal to the impingement times. As the hysteresis on the coating surface reaches a plateau, the coating is totally failed because surface topology at this stage has been considerably changed shown by Fig. 7(c) and Fig. 7(d) and the coating has lost most hydro-/ice-phobicity. The plateau of the curve also can be understood that current impact pressure has gradually damaged the surface to the total failure and the rest material can stand the impact stress very well. This total failure is the same as the fracture of member in conventional material fatigue.

Slot et al. uses Miner theory to give a prediction of coating lifetime [7]. Miner theory is used to give prediction of coating surface, but it needs plenty of experimental data support because of its empirical nature and loading interactions is not considered by it. Therefore, Miner theory is limited to this study because the mechanical properties of coating surface is not well known, and more than one stress will be considered for the cumulative damage of coating surface. However, Corten-Dolan's fatigue theory includes both stress-dependence and interaction effects. The introduction of interaction effects leads to the possibility of predictions that differs from Miner theory and it also can reduce the amount of needed data. Corten and Dolan assume that the damage of highest stress in a spectrum will affect the growth of damage at other lower stress amplitudes. The Corten-Dolan damage formula is given by:

$$D = mrN^a \tag{10}$$

m is the number of nuclei and a is damage propagation exponent. m and r has a relationship to the stress level but damage exponent a is proved to be independent of stress level but change with different material [26, 27]. rN^a is the damage from one nuclei and multiplication with the number of nuclei m is the total damage. The number of nuclei is assumed to be a constant for all stress level in this experiment to simplify the problem. Corten and Dolan found an experimental relation between the stress ratio and expansion rate ratio by a material property d expressed as:

$$(\frac{r_1}{r_2})^{1/a} = (\frac{\sigma_1}{\sigma_2})^d \tag{11}$$

S-N curve is a plot of stress (S) against the number of stress cycle to failure (N) widely used in typical fatigue theory. Base on equation (11), Corten and Dolan suggest a modification of *S-N* diagram to be determined by one line in the entire region given by [28]

$$N = N_1(\frac{\sigma}{\sigma_1})^d \tag{12}$$

N_1 is the number of stress cycle endured at the stress σ_1. For a stress spectrum, the failure can happen as:

$$\sum_i (\frac{n_i}{N_1})(\frac{\sigma}{\sigma_1})^d = 1 \tag{13}$$

n_i is the number of stress cycle endured at the stress σ_i and N_1 is the lifetime under maximum stress σ_1 in a stress spectrum. The damage degree of water-hammer impact, Rayleigh wave and dynamic pressure are assumed to be D_1, D_2 and D_3, respectively and can be given by:

$$\begin{cases} D_1 = \dfrac{N'}{N_1} \\ D_2 = \int_{r'}^{r_\infty} \dfrac{N'}{N_1} \left(\dfrac{P_w(r)}{P_w}\right)^d dr \\ D_3 = \dfrac{N}{N_1} \left(\dfrac{P_d}{P_w}\right)^d \end{cases} \tag{14}$$

r_∞ is the radius of area where Rayleigh wave's amplitude reduces to dynamic pressure P_d at the edge. Selecting dynamic pressure as the far field pressure is that dynamic pressure will be frequently applied to the surface (more than 10Hz) so that pressure lower than it can be enveloped.

Applying equation (1~6) to equation (14), the total damage level can be expressed as

$$D = K \cdot LWC \cdot t \cdot v^3 \cdot \left[1 + \frac{4}{4-d} \left(\left(\frac{v}{c}\right)^{(d-4)/2} - 1 \right) + \left(\frac{v}{c}\right)^{(d/2)-2} \right] \tag{15}$$

The first term in the polynomial represents the damage of water impact, the second term is for Rayleigh wave and the final one is for dynamic pressure. K is a constant term for a specific material and has effect to shrink the difference between coating fatigue model and typical fatigue model. The importance of each stress for coating damage can be analyzed by equation (15) with different material property constant d. If the lifetime of one case has been got, the lifetime with different parameters can be estimated by:

$$N = \frac{LWC_1 \cdot f(v_1)}{LWC \cdot f(v)} N_1 \tag{16}$$

Subscript 1 represents the reference case parameter and $f(v)$ is the last polynomial term in equation (15).

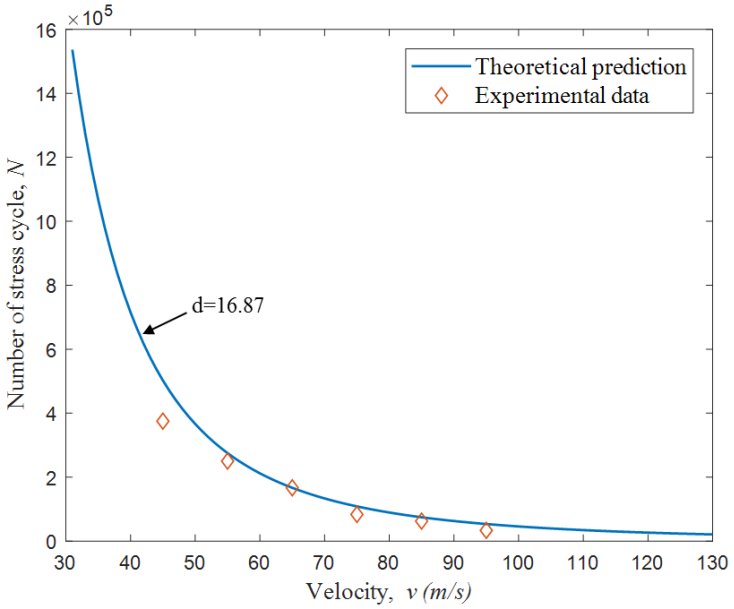

Figure 9: Predicted lifetime and experimental lifetime curve

The case with 65m/s wind velocity is selected as the reference one to predict lifetime of other cases. Figure 9 shows predicted lifetime and it fits well with experimental lifetime of superhydrophobic coating. The material constant of tested superhydrophobic surface is determined by experimental data, d=16.87. Experiment with a wind velocity of 45m/s shows over-predicted lifetime mainly because the stress-nuclei relationship is ignored as the model is developed. Low stress level can contribute to the less nuclei generation. Taking d back to equation (15) can compare the damage of each stress. Assuming impact velocity is 65m/s and sound speed in coating is 1498m/s (aluminum substrate sound

speed), the value of first term is 1, second term is 0.31 and the third term is 10^{-9}. It can show that the velocity polynomial's first and second term corresponding to water hammer pressure and Rayleigh wave damage are much bigger than the third term which reveals that water hammer pressure and Rayleigh wave is the most dominant reason for the coating damage. Thomas et al. successfully use the water hammer theory to explain the material mass loss problem as they study the metal surface failure by droplets erosion [11]. As for the coating lifetime prediction for the aircraft, assuming a plane is moving with a velocity of 150m/s, the critical impingement times can be given by equation (16) which is about 15000 times. If the $LWC = 0.05 g/m^3$ which is the *LWC* of the fog, the coating working duration is estimated by equation (6) which is approximately 7.5 hours. After this period, although coated surface may still perform better than the substrate, it cannot effectively work for anti-icing or water repellence.

V. Conclusions

The durability of a superhydrophobic coating surface is tested by droplet erosion with different impact velocities and impingement times. The hydrophobicity and icephobicity characteristics including contact angle, hysteresis and ice adhesion strength are measured. Contact angle and hysteresis can be seen a drop with increase of impingement times and impact velocity. Hysteresis can reach a plateau until a critical impingement times which decreases with increment of impact velocity. Ice adhesion strength is observed to have a rise with higher hysteresis value which can be predicted by fracture mechanics theory. Therefore, such plateau is regarded as the failure of the coating surface because the superhydrophobic coating surface has lost its hydrophobicity and icephobicity characteristics. The source of damage is analyzed and water hammer pressure, Rayleigh wave and dynamic pressure are three main representative stress during the impact of water droplet. The lifetime prediction approach of the coating is developed based on Corten-Dolan fatigue theory described as a function of the impact velocity and *LWC* as well as Coating life is predicted well by current model.

Acknowledgements

The research work is partially supported by Iowa Space Grant Consortium (ISGC) Base Program for Aircraft Icing Studies, National Aeronautics and Space Administration (NASA) with the grant numbers of NNX16AN21A and NNX12C21A, and National Science Foundation (NSF) under award numbers of CBET1064196 and CBET1435590. The authors gratefully acknowledge Prof. Juan Ren at Iowa state university for use of the AFM measurements.

Reference

[1] Liu, Y., Li, L., and Hu, H., "An Experimental Study on the Transient Heat Transfer and Dynamic Ice Accretion Process over a Rotating UAS Propeller," *9th AIAA Atmospheric and Space Environments Conference*, 2017.

[2] Liu, Y., Li, L., Ning, Z., Tian, W., and Hu, H., "Experimental Investigation on the Dynamic Icing Process over a Rotating Propeller Model," *AIAA Journal of Power and Propulsion*, 2018, pp. 1–15.

[3] Zhuo, Y., Håkonsen, V., He, Z., Xiao, S., He, J., and Zhang, Z., "Enhancing the Mechanical Durability of Icephobic Surfaces by Introducing Autonomous Self-Healing Function," *ACS Applied Materials & Interfaces*, 2018.

[4] Feng, B. L., Li, S. H., Li, Y. S., Li, H. J., Zhang, L. J., Zhai, J., Song, Y. L., Liu, B. Q., Jiang, L., Feng, L., Li, S. H., Li, Y. S., Li, H. J., Zhang, L. J., Zhai, J., Song, Y. L., Liu, B. Q., Jiang, L., and Zhu, D. B., "Super-hydrophobic surfaces: From natural to artificial," *Advanced Materials*, vol. 14, 2002, pp. 1857–1860.

[5] Hu, D. L., Chan, B., and Bush, J. W. M., "The hydrodynamics of water strider locomotion," *Nature*, vol. 424, 2003, pp. 663–666.

[6] Simpson, J. T., Hunter, S. R., and Aytug, T., "Superhydrophobic materials and coatings: A review," *Reports on Progress in Physics*, vol. 78, 2015.

[7] Slot, H. M., Gelinck, E. R. M., Rentrop, C., and Van der Heide, E., "Leading edge erosion of coated wind turbine blades: Review of coating life models," *Renewable Energy*, vol. 80, 2015, pp. 837–848.

[8] Ishizaki, T., Masuda, Y., and Sakamoto, M., "Corrosion resistance and durability of superhydrophobic surface formed on

magnesium alloy coated with nanostructured cerium oxide film and fluoroalkylsilane molecules in corrosive NaCl aqueous solution," *Langmuir*, vol. 27, 2011, pp. 4780–4788.

[9] Xiu, Y., Liu, Y., Hess, D. W., and Wong, C. P., "Mechanically robust superhydrophobicity on hierarchically structured Si surfaces," *Nanotechnology*, vol. 21, 2010.

[10] Ghidaoui, M. S., Zhao, M., McInnis, D. A., and Axworthy, D. H., "A Review of Water Hammer Theory and Practice," *Applied Mechanics Reviews*, vol. 58, 2005, p. 49.

[11] Thomas, G. P., and Brunton, J. H., "Drop Impingement Erosion of Metals," *Proceedings of the Royal Society A: Mathematical, Physical and Engineering Sciences*, vol. 314, 1970, pp. 549–565.

[12] Farhadi, S., Farzaneh, M., and Kulinich, S. A., "Anti-icing performance of superhydrophobic surfaces," *Applied Surface Science*, vol. 257, 2011, pp. 6264–6269.

[13] Wang, Y., Xue, J., Wang, Q., Chen, Q., and Ding, J., "Verification of icephobic/anti-icing properties of a superhydrophobic surface," *ACS Applied Materials and Interfaces*, vol. 5, 2013, pp. 3370–3381.

[14] "SUPERHYDROPHOBIC SURFACES TO RESIST DROPLET," 2013.

[15] Soto, D., De Larivière, A. B., Boutillon, X., Clanet, C., and Quéré, D., "The force of impacting rain," *Soft Matter*, vol. 10, 2014, pp. 4929–4934.

[16] Lesser, M. B., "Analytic Solutions of Liquid-Drop Impact Problems," *Proceedings of the Royal Society A: Mathematical, Physical and Engineering Sciences*, vol. 377, 1981, pp. 289–308.

[17] Meuler, A. J., Smith, J. D., Varanasi, K. K., Mabry, J. M., McKinley, G. H., and Cohen, R. E., "Relationships between water wettability and ice adhesion," *ACS Applied Materials and Interfaces*, vol. 2, 2010, pp. 3100–3110.

[18] Beeram, P. S. R., "Characterization of ice adhesion strength over different surfaces pertinent to aircraft anti-/de-icing," *Graduate Theses and Dissertations*, 2017.

[19] Fujisawa, N., Takano, S., Fujisawa, K., and Yamagata, T., "Experiments on liquid droplet impingement erosion on a rough surface," *Wear*, vol. 398–399, 2018, pp. 158–164.

[20] Chen, L., Xiao, Z., Chan, P. C. H., Lee, Y. K., and Li, Z., "A comparative study of droplet impact dynamics on a dual-scaled superhydrophobic surface and lotus leaf," *Applied Surface Science*, vol. 257, 2011, pp. 8857–8863.

[21] Sun, X., Damle, V. G., Liu, S., and Rykaczewski, K., "Bioinspired Stimuli-Responsive and Antifreeze-Secreting Anti-Icing Coatings," *Advanced Materials Interfaces*, vol. 2, 2015, pp. 25–27.

[22] Zheng, S., Li, C., Fu, Q., Hu, W., Xiang, T., Wang, Q., Du, M., Liu, X., and Chen, Z., "Development of stable superhydrophobic coatings on aluminum surface for corrosion-resistant, self-cleaning, and anti-icing applications," *Materials and Design*, vol. 93, 2016, pp. 261–270.

[23] Hejazi, V., Sobolev, K., and Nosonovsky, M., "From superhydrophobicity to icephobicity: Forces and interaction analysis," *Scientific Reports*, vol. 3, 2013.

[24] He, Z., Xiao, S., Gao, H., He, J., and Zhang, Z., "Multiscale crack initiator promoted super-low ice adhesion surfaces," *Soft Matter*, vol. 13, 2017, pp. 6562–6568.

[25] Petrenko, V. F., "Study of the Surface of Ice, Ice/Solid and Ice/Liquid Interfaces with Scanning Force Microscopy," *The Journal of Physical Chemistry B*, vol. 101, 1997, pp. 6276–6281.

[26] Kaechele, L., *Review and analysis of cumulative-fatigue-damage theory*, 1963.

[27] Rao, J. S., Pathak, A., and Chawla, A., "Blade Life: A Comparison by Cumulative Damage Theories," *Journal of Engineering for Gas Turbines and Power*, vol. 123, 2001, pp. 886–892.

[28] Zhu, S. P., Huang, H. Z., Liu, Y., He, L. P., and Liao, Q., "A practical method for determining the Corten-Dolan exponent and its application to fatigue life prediction," *International Journal of Turbo and Jet Engines*, vol. 29, 2012, pp. 79–87.